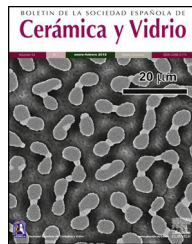




BOLETIN DE LA SOCIEDAD ESPAÑOLA DE
Cerámica y Vidrio

www.elsevier.es/bsecv



Original

The effect of particle size and phosphorous content in biomineralization media on *in vitro* bioactivity of monticellite based ceramic powders obtained from boron derivative waste



Levent Koroglu^a, Ceren Peksen^{b,*}

^a Department of Materials Science and Engineering, Eskisehir Technical University, Eskisehir 26555, Turkey

^b Department of Ceramic and Glass, Ondokuz Mayis University, Samsun 55100, Turkey

ARTICLE INFO

Article history:

Received 9 August 2019

Accepted 23 January 2020

Available online 14 February 2020

Keywords:

Monticellite

Bioactivity

Particle size

Crystallization

Boron derivative waste

ABSTRACT

The effect of particle size and phosphorous content in biomineralization media on *in vitro* bioactivity of monticellite based ceramic powders was investigated. Monticellite based ceramic powder was synthesized at 800 °C for 4 h using boron derivative waste. Monticellite based ceramic powder, comprising monticellite, akermanite, diopside, calcium magnesium borate and zeolite LTA crystalline phases, was crushed and then ball-milled for optimized time to obtain lowest average particle size and the narrowest particle size distribution. *In vitro* bioactivity of both coarse (d_{10} : 0.5 μm , d_{50} : 3.0 μm , d_{90} : 42 μm) and fine (d_{10} : 0.5 μm , d_{50} : 1.4 μm , d_{90} : 4.8 μm) wafers was determined by incubation in Lactated Ringer's Solution and Human Blood Plasma for 1, 3, 5, 7, 14, 21 and 28 days at $36.5 \pm 0.5^\circ\text{C}$. The obtained results exhibited that calcite (CaCO_3) layer after immersion in Lactated Ringer's Solution and bone-like apatite layer after immersion in Human Blood Plasma were formed on the surface of coarse and fine wafers. The presence of phosphorus in biomineralization media is necessary for apatite formation. The increment of surface roughness favors homogeneous nucleation, and fasten nucleation and growth kinetics of precipitation. As a result, the bioactive characteristic of monticellite based ceramic powder could be governed by the particle size.

© 2020 SECV. Published by Elsevier España, S.L.U. This is an open access article under the CC BY-NC-ND license (<http://creativecommons.org/licenses/by-nc-nd/4.0/>).

El efecto del tamaño de partícula y el contenido de fósforo en los medios de biomineralización sobre la bioactividad *in vitro* de los polvos cerámicos a base de monticellita obtenidos a partir de residuos de derivados de boro

RESUMEN

Se investigó el efecto del tamaño de partícula y el contenido de fósforo en los medios de biomineralización sobre la bioactividad *in vitro* de polvos cerámicos a base de monticellita.

Palabras clave:

Monticellita

* Corresponding author.

E-mail address: cpeksen@omu.edu.tr (C. Peksen).

<https://doi.org/10.1016/j.bsecv.2020.01.007>

0366-3175/© 2020 SECV. Published by Elsevier España, S.L.U. This is an open access article under the CC BY-NC-ND license (<http://creativecommons.org/licenses/by-nc-nd/4.0/>).

Bioactividad
Tamaño de partícula
Cristalización
Residuos derivados de boro

El polvo cerámico a base de monticellita se sintetizó a 800 °C durante 4 h utilizando residuos de derivados de boro. El polvo cerámico a base de monticellita, que comprende monticellita, akermanita, diópsido, borato de calcio y magnesio y fases cristalinas de zeolita LTA se trituró, y luego se molió con bola durante un tiempo optimizado para obtener el tamaño de partícula promedio más bajo y la distribución de tamaño de partícula más estrecha. La bioactividad *in vitro* de obleas gruesas (d_{10} : 0.5 μm , d_{50} : 3.0 μm , d_{90} : 42 μm) y finas (d_{10} : 0.5 μm , d_{50} : 1.4 μm , d_{90} : 4.8 μm) se determinó mediante incubación en solución de Ringer lactato y plasma sanguíneo humano durante 1, 3, 5, 7, 14, 21 y 28 días a 36,5 ± 0,5 °C. Los resultados obtenidos mostraron que la capa de calcita (CaCO_3) después de la inmersión en la solución de Ringer lactato y la capa de apatita similar a un hueso después de la inmersión en plasma sanguíneo humano se formaron en la superficie de obleas gruesas y finas. La presencia de fósforo en los medios de biominerilación es necesaria para la formación de apatita. El incremento de la rugosidad de la superficie favorece la nucleación homogénea y fija la cinética de nucleación y crecimiento de la precipitación. Como resultado, la característica bioactiva del polvo cerámico a base de monticellita podría estar gobernada por el tamaño de partícula.

© 2020 SECV. Publicado por Elsevier España, S.L.U. Este es un artículo Open Access bajo la licencia CC BY-NC-ND (<http://creativecommons.org/licenses/by-nc-nd/4.0/>).

Introduction

Bioactivity is a crucial characteristic for bone grafts which leads the formation of a bone-like apatite layer at the tissue-implant interface upon immersion in biological fluids. The formed bone-like apatite layer provides osteoconductivity and then chemically stable and strong implant-bone bond. For this reason, bioactive ceramics have been widely used as bone graft substitutes in the last decades due to their high biocompatibility and also, high bioactivity [1–7]. Among bioactive ceramics, monticellite (CaMgSiO_4) bioactive ceramics have received much attention as a bone void filler and a coating material on Ti-6Al-4V alloy for orthopedic applications owing to not only high biocompatibility and high bioactivity characteristics and also, superior mechanical and thermal properties compared to hydroxyapatite (HAp), akermanite ($\text{Ca}_2\text{MgSi}_2\text{O}_7$) and merwinite ($\text{Ca}_3\text{MgSi}_2\text{O}_8$) bioactive ceramics [7–13].

Turkey has almost 72% of the boron reserves in the worldwide. During the refinement of tincal minerals to obtain borax pentahydrate, boron derivative waste are generated in large quantities (hundreds of thousands of tons per year) in Kırka Plant of Eti Mine Works General Directorate, in Eskişehir/Turkey. The deposition of boron derivative waste causes costly storage problems and serious environmental pollutions [14]. For this reason, in the previous study, monticellite based bioactive ceramic powders have been synthesized in an eco-friendly and cost-effective way using boron derivative waste, provided from Kırka Plant of Eti Mine Works General Directorate [15]. Until today, monticellite bioactive ceramics

have been produced only by the sol-gel method [8,10–12]. It was the first study [15] in which monticellite has been obtained by solid-state synthesis method. Moreover, *in vitro* bioactivity and *in vitro* cytotoxicity of synthesized monticellite based ceramic powders have been determined [16,17]. However, there is still a shortage in the literature for a detailed investigation on *in vitro* bioactivity characteristic of monticellite based ceramic powders because the obtained data after only 15 and 25 days incubation in SBF was not comprehensive in previous study [16].

The bone-like apatite formation is an ion-exchange reaction between the bioactive implant and surrounding body fluid and can be considered as liquid-phase synthesis including dissolution and re-precipitation stages [18,19]. The bone-like apatite formation can be enhanced by increasing surface area of implants results in higher ion-exchange rate, while surface roughness contributes to the attachment, proliferation and osteoblast differentiation [18]. It is known that the bulk (mass) density, pore properties, specific surface area, and surface roughness are dominated by particle size distribution [20]. In the light of that, surface features governing ion-exchange rate and nucleation and growth mechanisms for apatite layer formation could be tuned by particle size distribution.

To our best knowledge, there are a few types of research on the literature which is focused on the effect of particle size on *in vitro* bioactivity of ceramics or ceramic matrix composites. Chatzistavrou et al. [21] investigated the influence of particle size on the bioactive behavior of bioactive $\text{SiO}_2\text{--Na}_2\text{O}\text{--CaO}\text{--P}_2\text{O}_5$ glass system. They found that the bioactive response of $\text{SiO}_2\text{--Na}_2\text{O}\text{--CaO}\text{--P}_2\text{O}_5$ glass system becomes

Table 1 – Ion concentrations of Human Blood Plasma (HBF), Simulated Body Fluid (SBF) and Lactated Ringer's solution (LRS).

Ion concentration (mM)	Na^+	K^+	Mg^{2+}	Ca^{2+}	Cl^-	HCO_3^-	HPO_4^{2-}	SO_4^{2-}	Na-lactate
Human Blood Plasma	142.0	5.0	1.5	2.5	103.0	27.0	1.0	0.5	–
Original SBF	142.0	5.0	1.5	2.5	148.8	4.2	1.0	0	–
LRS	130.7	4.02	–	1.4	109.5	–	–	–	22

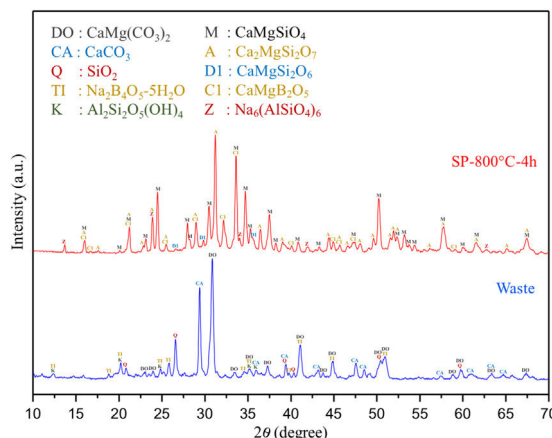


Fig. 1 – Comparative XRD patterns of boron derivative waste and synthesized monticellite based ceramic powder at 800 °C for 4 h (SP-800 °C-4 h).

better with the increase of particle size of powders up to 80 µm, while there is no further improvement with particle size >80 µm. The reason was attributed that the total surface area seems to decrease asymptotically with the increase of the particle size. Nevertheless, comprehensive research focused on the effect of particle size on in vitro bioactivity of a bio-ceramic is needed to make a contribution to the existing literature.

Nowadays, Simulated Body Fluid (SBF) was widely used by the researchers as a biominerization media for in vitro bioactivity assessments. However, the requirement of a high number of reagents, precise pH adjustment and long procedure time, makes the preparation of SBF solutions painful. Lactated Ringer's Solution (LRS) is widely used in hospitals due to no adverse effects reported in patients [22]. Moreover, LRS has a low cost and can be supplied from the pharmacy. At this

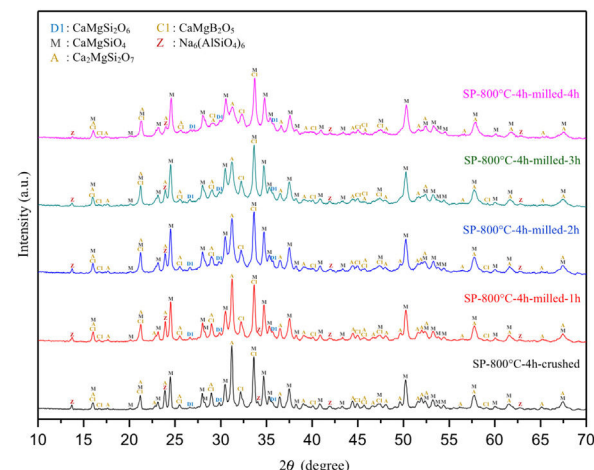


Fig. 3 – Comparative XRD patterns of crushed SP-800 °C-4 h and ball-milled SP-800 °C-4 h powders for 1, 2, 3 and 4 h using 1 wt.% SA.

point, LRS has been attracted for the usage as biominerization media for in vitro bioactivity assessments. However, LRS is lack of some ions such as Mg²⁺, HCO₃⁻, HPO₄²⁻ and SO₄²⁻. Especially, the absence of hydrogen phosphate could be critical for the precipitation of Ca-P based bone-like hydroxyapatite layer on the surface.

Therefore, the aim of the study was the investigation of the effect of particle size and phosphorous content in biominerization media on in vitro bioactivity of monticellite based ceramic powders. Firstly, the solid-state synthesis of MBCPs carried out using boron derivative waste. Secondly, the average particle size was reduced, and particle size distribution was narrowed by ball-milling of synthesized powder along with the optimization of milling time. Finally, the bone-like apatite formation ability of both coarse and fine monticellite based



Fig. 2 – Images of (a) synthesized powder at 800 °C for 4 h (SP-800 °C-4 h), (b) SP-800 °C-4 h-crushed and (c) SP-800 °C-4 h-milled-2 h-1 wt.% SA.

Table 2 – Three characteristic particle diameters of crushed and ball-milled monticellite based ceramic powders.

Sample code	d(0.1) (µm)	d(0.5) (µm)	d(0.9) (µm)	Mean crystallite size of monticellite (nm)
Boron derivative waste	0.414	0.823	2.776	–
SP-800 °C-4 h-crushed	0.567	3.091	42.856	34.71
SP-800 °C-4 h-milled-1 h-1 wt.% SA	0.604	1.517	5.216	31.36
SP-800 °C-4 h-milled-2 h-1 wt.% SA	0.574	1.463	4.813	30.51
SP-800 °C-4 h-milled-3 h-1 wt.% SA	0.618	1.621	5.481	46.26
SP-800 °C-4 h-milled-4 h-1 wt.% SA	0.603	2.002	8.894	34.97

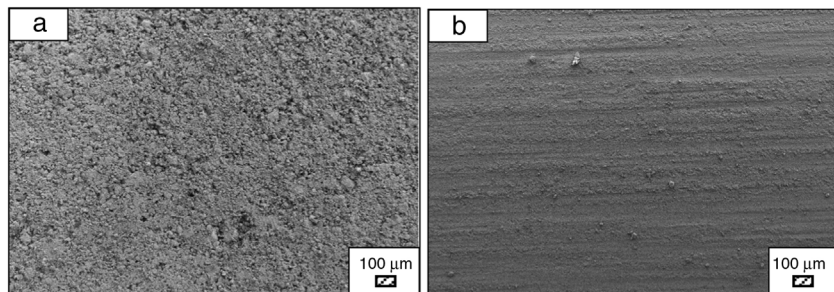


Fig. 4 – SEM micrographs (SE mode) of the surface of (a) coarse (SP-800 °C-4 h-crushed) wafer and (b) fine (SP-800 °C-4 h-milled-2 h) wafer before incubation (100×).

Table 3 – The surface roughness profile of coarse and fine wafers.

Sample	R _a (μm)	R _Z (μm)	R _{max} (μm)
Coarse wafer	1.97	16.44	20.61
Fine wafer	1.22	7.39	10.38

ceramic powders was investigated by the immersion in Lactated Ringer's Solution and Human Blood Plasma for various periods.

Experimental procedure

Preparation of monticellite based ceramic powder

Boron derivative waste supplied from Kırka Plant of Eti Mine Works General Directorate was used as starting material. The solid-state synthesis of monticellite (CaMgSiO_4) based ceramic powder carried out by the heat-treatment of boron derivative waste at 800 °C for 4 h in an electrically heated furnace (KRC Lab. Eq.) under atmospheric pressure. The heating rate was kept at 10 °C/min. Following the heating cycle, the refractory plate was taken out and allowed to be quenched to room temperature in air. The purpose of rapid cooling lies on the decreasing of crystallinity degree which leads to higher dissolution rate and consequently, the faster ion exchange contributes to bone-like apatite formation ability [23]. The critical process parameters (800 °C, 4 h, 10 °C/min) had been optimized to obtain maximum monticellite phase content in the synthesized powder during prior systematic study [15].

After the solid-state synthesis, the obtained powder was crushed and ground to below 63 μm. The qualitative phase analysis both of boron derivative waste and monticellite based ceramic powder was performed using X-Ray Diffractometer (XRD, Miniflex 600, Rigaku) with a scan speed of 0.5°/min in the 2θ range of 10–70°. The detailed characteristic knowledge (XRF, TG–DTA, FTIR, SEM) of boron derivative waste and MBCP could be obtained from the prior study [15].

Particle size reduction of monticellite based ceramic powders

In order to reduce the particle size of synthesized MBCP at 800 °C for 4 h (SP-800 °C-4 h), the synthesized powder was

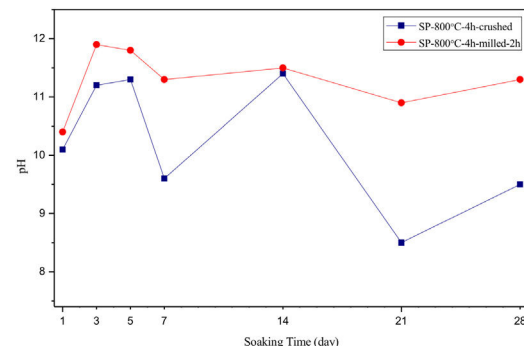


Fig. 5 – pH values of LRS with respect to immersion time.

firstly crushed in agate mortar and secondly ball-milled under liquid-free environment using a planetary ball mill (Pulverisette 6, Fritsch) at rotational speed of 400 rpm in ZrO_2 media (80 ml bowl volume and 10 mm ball diameter, Fritsch). In the planetary ball mill, crushing and milling are carried out by the combination of impact and shear stresses. Along with the fracture of a solid, energy as heat is released from fracture and it is necessary for creating additional surface area [24,25]. The particle size distribution and the degree of disorder of milled powders depend on the milling conditions such as milling environment, the materials of milling tools, milling speed, milling time and ball-to-powder weight ratio [20]. Milling environment was preferred dry because dry milling is more efficient and could avoid the formation of hard agglomerates compared to wet milling. ZrO_2 milling media was selected due to its high wear resistance and biocompatible and bioinert characteristics [26]. The milling times were set to 1, 2, 3 and 4 h. The weight ratio of ball-to-powder kept 10:1. In order to reduce the caking problem, stearic acid ($(\text{CH}_3(\text{CH}_2)_{16}\text{COOH}$, Merck KGaA) was used as a deflocculant in 1 wt.% of charged powder, the direction of rotation of the planetary ball mill was reversed and the interior-wall of the bowl was scraped down per hour. Prior to the characterization of crushed and ball-milled MBCPs, stearic acid was removed away by heat-treatment at 400 °C for 2 h.

The particle size measurement of boron derivative waste, crushed powder, and ball-milled powders was accomplished by using laser diffraction particle size analyzer (Mastersizer 2000, Malvern Instruments) in deionized water. The qualita-

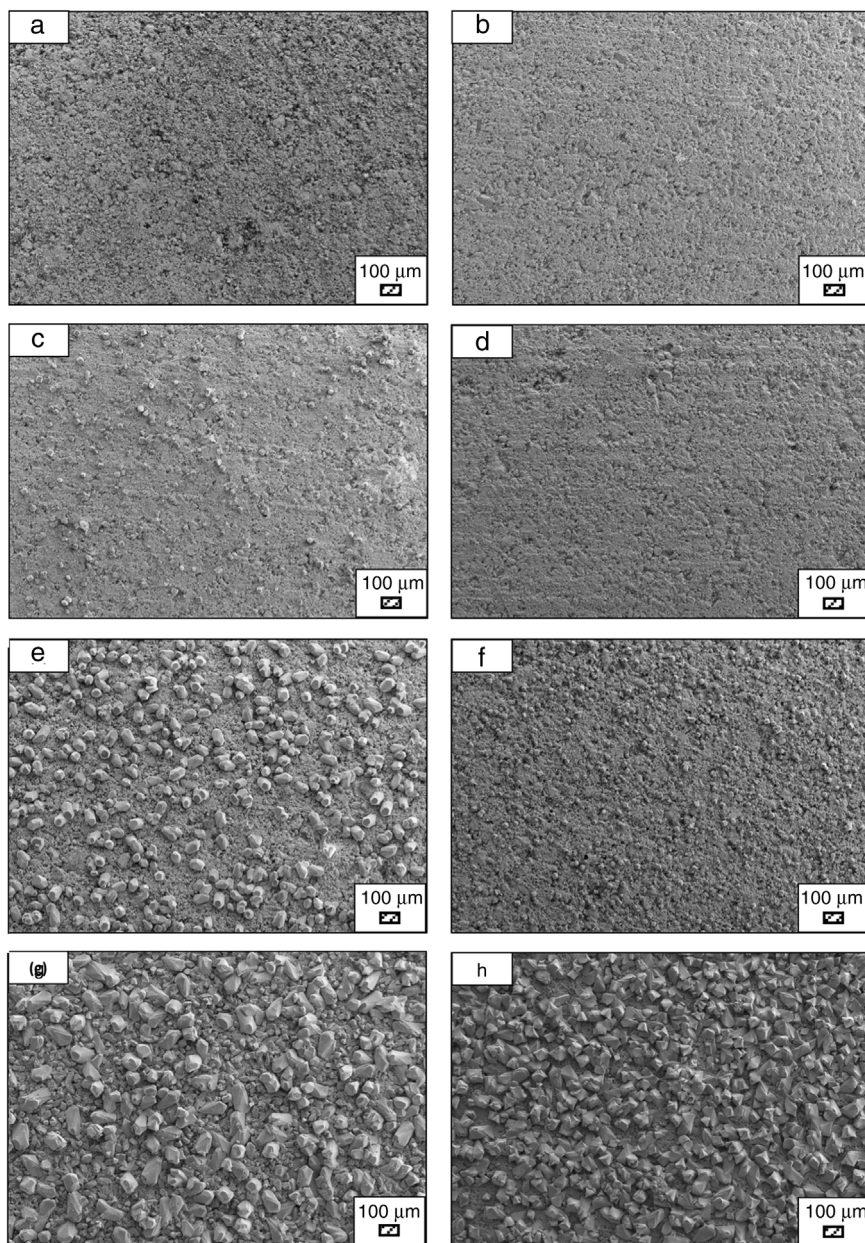


Fig. 6 – SEM micrographs of coarse wafer before (a) and after immersion in LRS for (b) 1 day; (c) 3 days; (d) 5 days; (e) 7 days; (f) 14 days; (g) 21 days and (h) 28 days (100 \times).

tive phase analysis of crushed and ball-milled powders was performed using XRD under the same conditions stated above. The mean crystallite size of monticellite in crushed powder and ball-milled powders was determined by Scherrer equation [27]. It was applied to the peaks of (120) and (222). The crushed powder in an agate mortar and ball-milled powders for each milling time were called SP-800 °C-4 h-crushed and SP-800 °C-4 h-milled-X h-Y wt.% SA where X donates milling time and Y stearic acid content.

In vitro bioactivity assessment of monticellite based ceramic powders

In the scope of the assessment of in vitro bioactivity, crushed SP-800 °C-4 h and SP-800 °C-4 h-milled-2 h were firstly compacted by uniaxial pressing. Secondly, obtained wafers with the dimensions of Ø13 × 3.5 mm² and the same mass were subjected to the cold isostatic press under 200 MPa. Finally, the wafers were divided into two equal pieces to

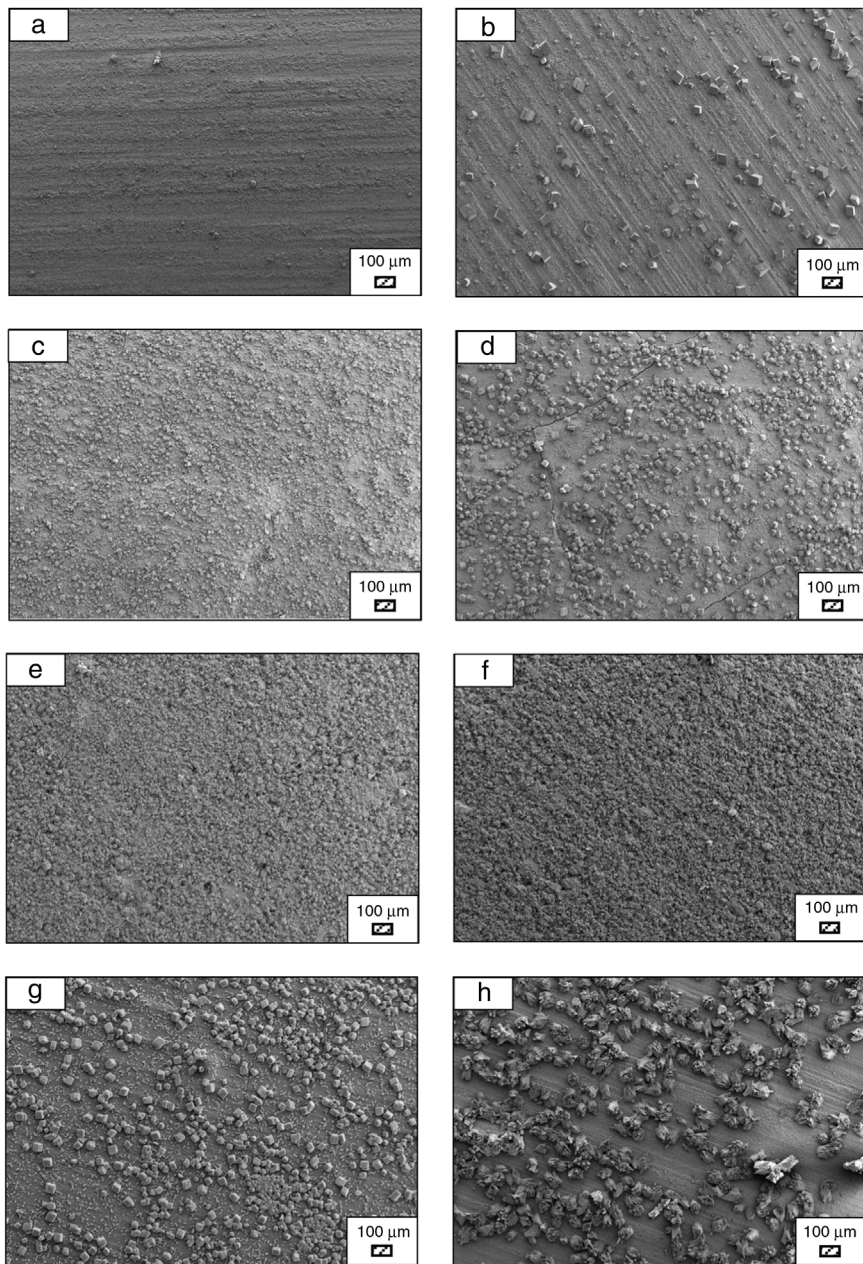


Fig. 7 – SEM micrographs of fine wafer before (a) and after immersion in LRS for (b) 1 day; (c) 3 days; (d) 5 days; (e) 7 days; (f) 14 days; (g) 21 days and (h) 28 days (100 \times).

examine the thickness of the formed bone-like apatite layer by SEM against the normalized cross-sectional area. The wafers were soaked in Lactated Ringer's Solution (LRS) supplied from a pharmacy, and Human Blood Plasma (HBP) supplied from a state hospital, for 1, 3, 5, 7, 14, 21 and 28 days at $36.5 \pm 0.5^\circ\text{C}$ using an incubator (KRC Lab. Eq.). Ion concentrations of Human Blood Plasma, Simulated Body Fluid (SBF) and Lactated Ringer's Solution are given in Table 1 [28]. The ratio of wafer surface area to solution volume was kept $0.1\text{ cm}^2/\text{ml}$. The wafers were taken out after selected incubation times, rinsed with deionized water and dried

for 24 h. The pH of solutions was measured before and after the assessment. The formation of a bone-like apatite layer on the surface of MBCP wafers was investigated using a scanning electron microscope (SEM, Supra 50VP, Zeiss) equipped with secondary electron (SE) and energy-dispersive X-ray spectroscopy (EDS) detectors (Oxford Instruments). Ca/P ratio on the surface of wafers incubated in HBP represented the average value which is determined by 5 different EDX point analysis of each wafer. The roughness of wafer surfaces was measured by a profilometer (MarSurf M 300, Mahr).

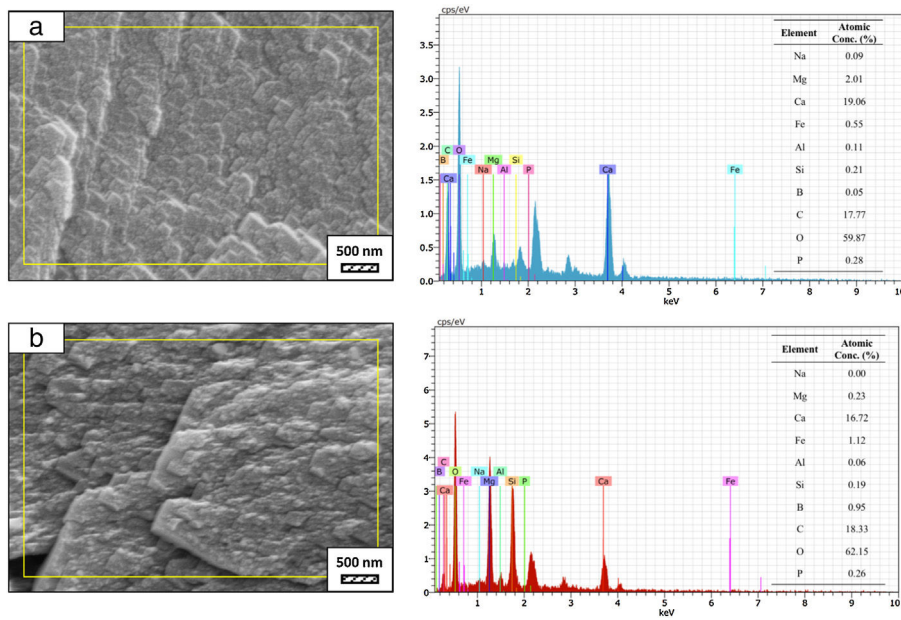


Fig. 8 – SEM micrographs and EDS analysis results of (a) coarse and (b) fine wafers soaked in LRS for 28 days.

Results and discussion

Phase evolution

Comparative XRD patterns of boron derivative waste and synthesized MBCP (SP-800 °C-4 h) are given in Fig. 1. XRD patterns showed that boron derivative waste was composed of dolomite ($\text{CaMg}(\text{CO}_3)_2$, ICDD 36-0426), calcite (CaCO_3 , ICDD 05-0586), quartz (SiO_2 , ICDD 87-2096), borax pentahydrate (tincalconite, $\text{Na}_2\text{B}_4\text{O}_7 \cdot 5\text{H}_2\text{O}$, ICDD 07-0277) and kaolinite ($\text{Al}_2\text{Si}_2\text{O}_5(\text{OH})_4$, ICDD 29-1488) crystalline phases. The synthesized MBCP comprised monticellite (CaMgSiO_4 , ICDD 76-0727), akermanite ($\text{Ca}_2\text{MgSi}_2\text{O}_7$, ICDD 83-1815), diopside ($\text{CaMgSi}_2\text{O}_6$, ICDD 78-1390), calcium magnesium borate (kurchatovite, CaMgB_2O_5 , ICDD 73-0618) and zeolite LTA (dehydrated sodalite, $\text{Na}_6(\text{AlSiO}_4)_6$, ICDD 42-0217). Monticellite, akermanite and calcium magnesium borate were found as major crystalline phases. It is known that Ca-Mg-Si based ceramics have high bioactivity. Also, it is reported that apatite formation ability of akermanite is higher than monticellite [10]. Considering this information, akermanite as a major phase will make a significant contribution to the apatite formation ability of monticellite based ceramic powders.

Effect of milling time on the particle size of monticellite based ceramic powders

Milling was performed using a planetary ball mill in order to obtain a particular particle size distribution. Images of synthesized powder at 800 °C for 4 h (SP-800 °C-4 h), crushed SP-800 °C-4 h in an agate mortar and ball-milled SP-800 °C-4 h for 2 h are given in Fig. 2. Three characteristic particle diameters of boron derivative waste, crushed SP-800 °C-4 h and ball-milled SP-800 °C-4 h for 1, 2, 3 and 4 h determined by laser diffraction particle size analysis and also mean crystallite size

of monticellite are given in Table 2. The waste consisted of fine particles with a narrow particle size range. The crushed powder after synthesis was composed of particles in a broad size range of 0.5–42.8 μm with an average size of 3.0 μm. It was associated with phase transformations in waste and particle agglomeration during heat treatment. With the increase of milling time up to 2 h, particle size range became narrower (0.5–4.8 μm) and the decreasing of both mean particle size (1.4 μm) and mean crystallite size of monticellite (30.51 nm) went further. However, the ball-milling for more than 2 h was inefficient to decrease the particle size range and crystallite size of monticellite. A noticeable broadening in particle size range and crystallite size of SP-800 °C-4 h-milled-3 h and SP-800 °C-4 h-milled-4 h was observed due to the agglomeration of powder particles and the growth of monticellite crystals. The optimal milling time was selected 2 h in order to obtain the lowest average particle size and the narrowest particle size distribution.

There is no more fast and easy way to get quick information on the milling progress than XRD that exposes the mean structural changes upon ball-milled powders for different milling times [20]. Comparative XRD patterns of crushed SP-800 °C-4 h and ball-milled SP-800 °C-4 h for 1, 2, 3 and 4 h using 1 wt.% of SA are given in Fig. 3. In similar to SP-800 °C-4 h, crushed and all milled powders include same crystalline phases such as monticellite, akermanite, and calcium magnesium borate in substantially and also, diopside and zeolite. It indicates that there is no contamination of ZrO_2 through milling media and no newly formed crystalline phases. Although XRD patterns of crushed SP-800 °C-4 h and milled SP-800 °C-4 h for 1 h are very similar, the peak intensities of akermanite relatively decreased for milled SP-800 °C-4 h for 2 h and this manner went further with the increment of milling time from 2 h to 4 h. The observed broad hump area under XRD patterns, especially between 27.5 and 37.5 diffraction angles, increased with milling time as an indication of decreased

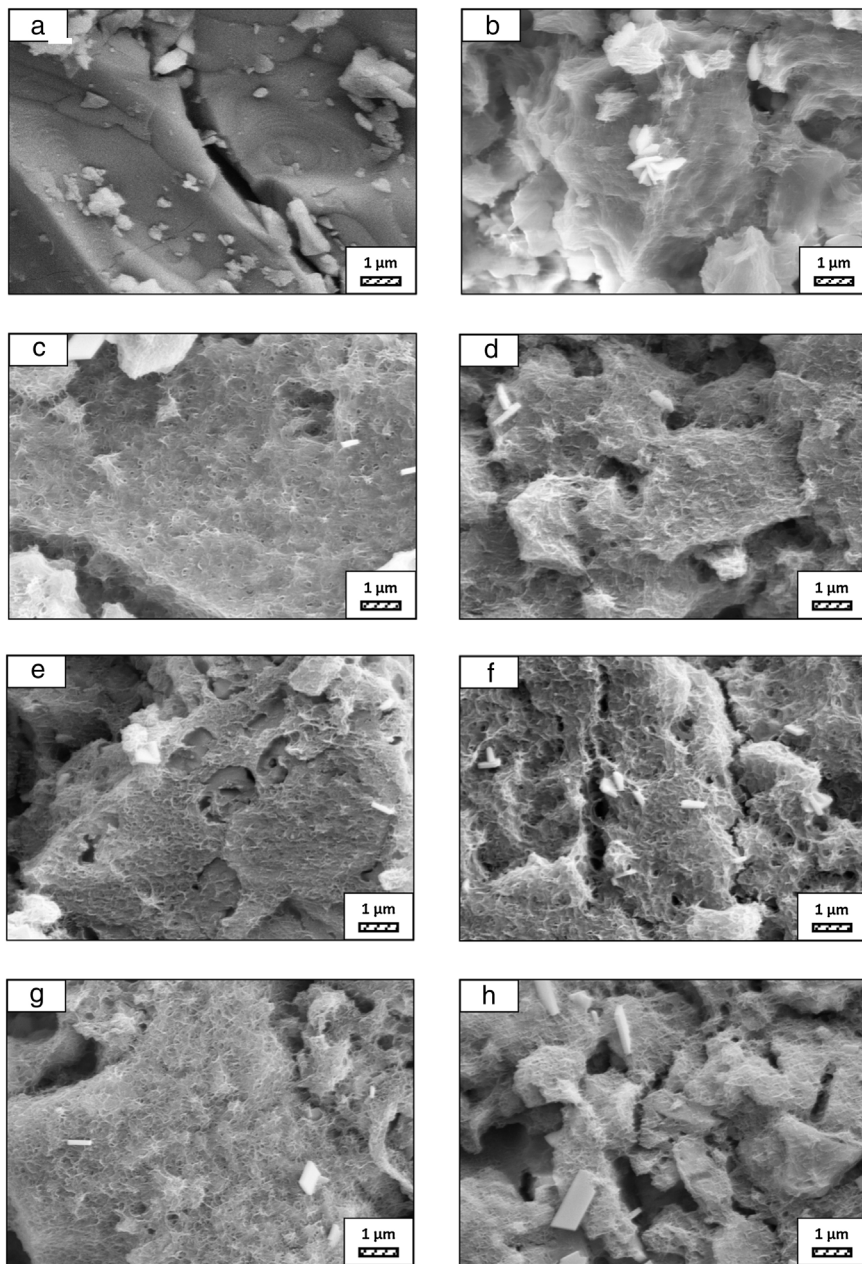


Fig. 9 – SEM micrographs of coarse wafer before (a) and after immersion in LRS for (b) 1 day; (c) 3 days; (d) 5 days; (e) 7 days; (f) 14 days; (g) 21 days and (h) 28 days (20,000 \times).

crystallinity degree. Akermanite passed from its starting long-range ordered structure to short-range ordered structure with repeated collisions. It is interesting that the amorphization was observed in akermanite while not in monticellite. It is attributed to the lower Mg/Ca ratio of akermanite (0.5) than that of monticellite (1). Mg–O bond energy was higher than that of the Ca–O bond. Thus, higher MgO content makes the crystal structure more stable [8,10]. Therefore, in contrast to monticellite, milling impact was able to affect the stability and crystallization of akermanite by breaking down its crystal structure.

Bone-like apatite formation ability of monticellite based ceramic powders

SEM images of the surface of coarse wafer (consisted of SP-800 °C-4 h-crushed powder) and fine wafer (consisted of SP-800 °C-4 h-milled-2 h) before incubation are given in Fig. 4. It can be observed in Fig. 4 that the surface of coarse wafer has relatively higher microporosity and higher surface roughness compare to fine wafer surface due to its broader particle size distribution. The surface roughness values of coarse and fine wafers, measured by a profilometer, are given in Table 3.

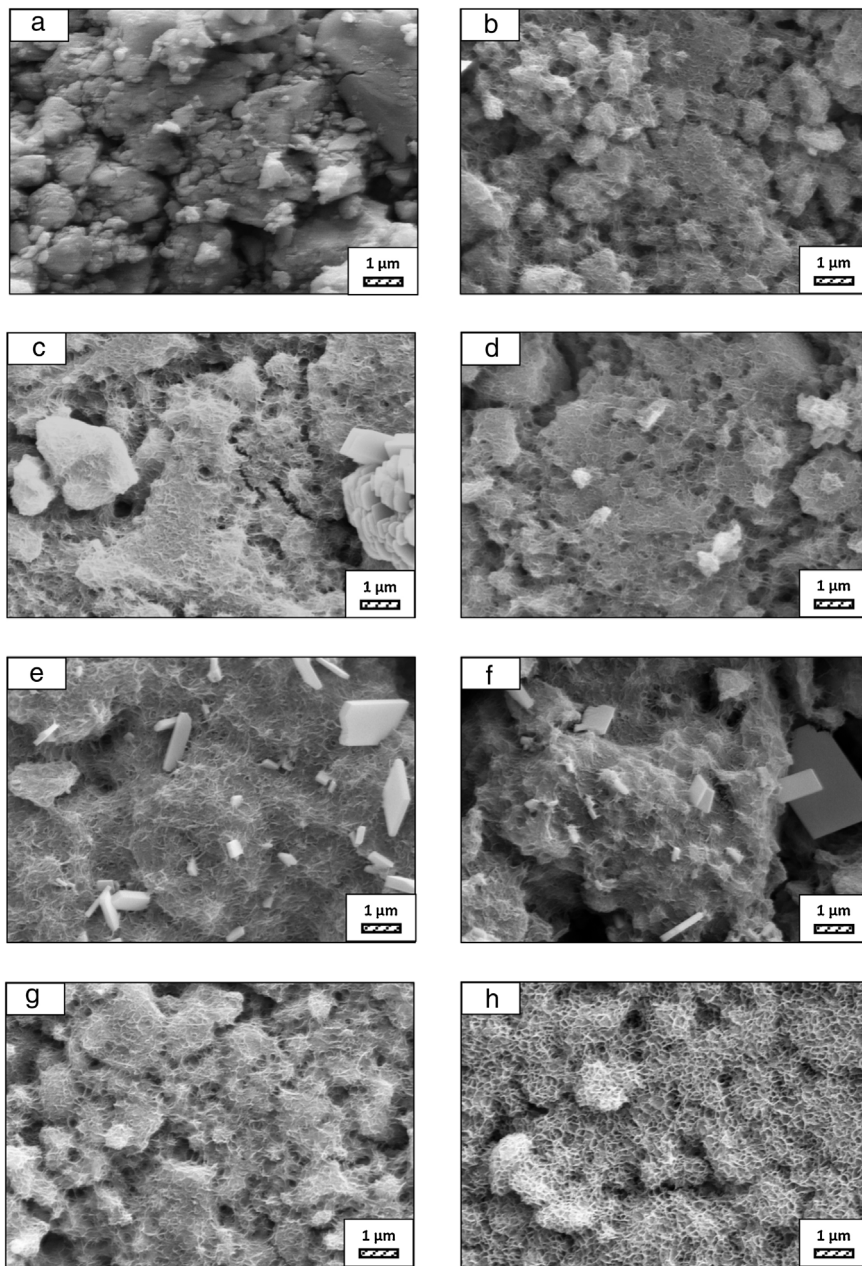


Fig. 10 – SEM micrographs of fine wafer before (a) and after immersion in LRS for (b) 1 day; (c) 3 days; (d) 5 days; (e) 7 days; (f) 14 days; (g) 21 days and (h) 28 days (20,000 \times).

According to the obtained results, the roughness of coarse wafer surface is higher than fine wafer surface. That theoretically refers to the higher specific surface area of coarse wafer surface. Inevitably, it is expect to affect the kinetics of apatite crystallization on wafer surfaces because high roughness increases sticking probability for atoms by providing higher number of nucleation sites [19].

In Lactated Ringer's Solution

The pH values of LRS with respect to immersion time are given in Fig. 5. SEM micrographs of coarse and fine wafers before and after 1, 3, 5, 7, 14, 21 and 28 days immersion in LRS are illustrated in Figs. 6 and 7. The obtained data showed that

the pH value of LRS for coarse wafers was found lower for all incubation period in comparison to fine wafers. It was associated to the higher surface roughness of coarse wafer which could result in a higher dissolution rate of alkali ions such as Ca^{2+} , Mg^{2+} , and Si^{4+} . It is observed on SEM micrographs that the precipitation occurred on the surfaces of both wafers. The number and size of precipitated particles on wafer surfaces increased with the increment of incubation time. These particles are more obvious on 7th days of incubation for coarse wafer and on the 1st day of incubation for fine wafer. In addition, precipitated particles are homogenously distributed on the surface of coarse wafer and the average size of large particles ($100 \mu\text{m}$) was found larger in comparison to fine wafer.

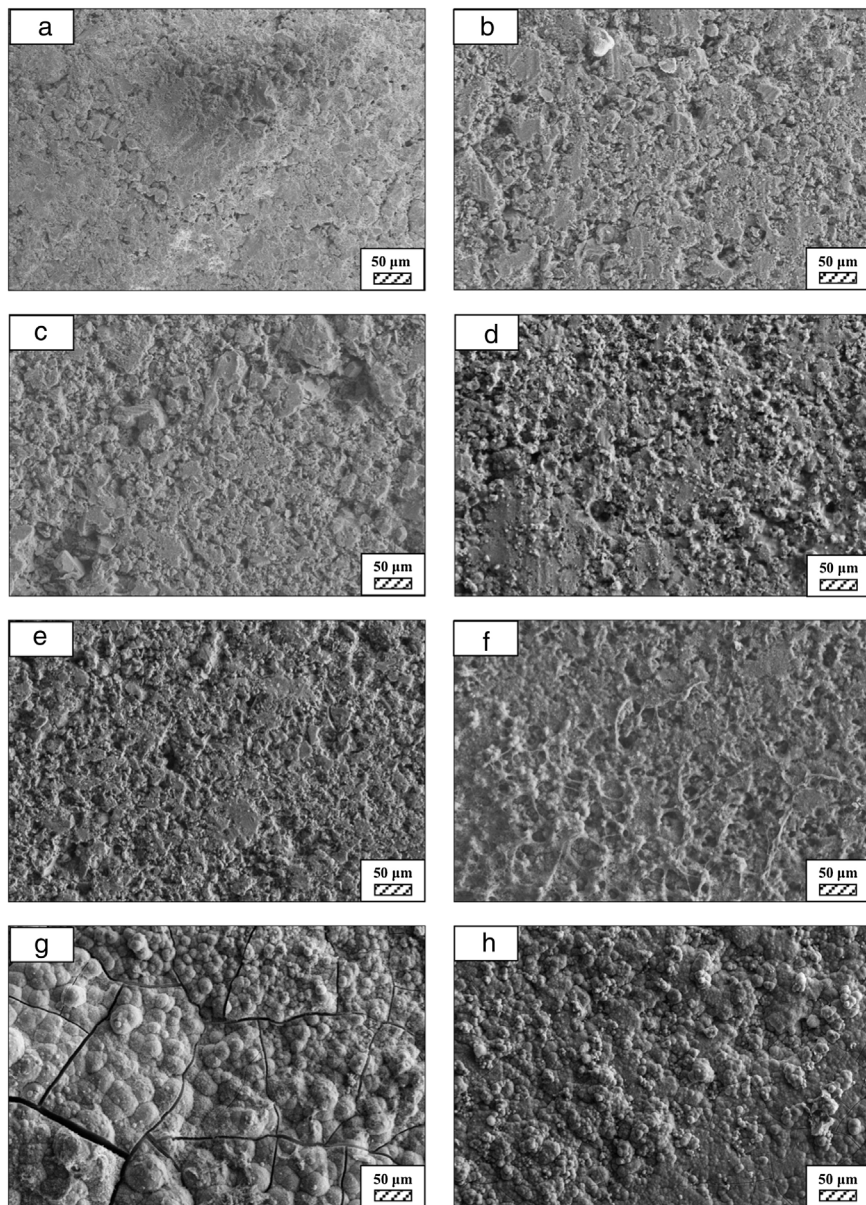


Fig. 11 – SEM micrographs of coarse wafer before (a) and after immersion in HBP for (b) 1 day; (c) 3 days; (d) 5 days; (e) 7 days; (f) 14 days; (g) 21 days and (h) 28 days (500 \times).

It was thought that a high number of nucleation sites on coarse wafer surface provided by surface roughness allows homogeneously distributed nucleation and high growth rate. For fine wafers, the precipitated particles larger than 50 μm could be seen at first even on the 1st day of incubation because all crystals had to located on a limited number of nucleation sites.

SEM micrographs and EDS analysis results of coarse and fine wafers soaked in LRS for 28 days are given in Fig. 8. EDS analysis results show that the composition of precipitated particles on wafer surfaces is calcite (CaCO_3). The variations in pH values (Fig. 5) could be caused by possible dissolution of precipitated calcite crystals. It is reported that calcite can be formed on the surface if biominerization media is lack of phosphorus (P) content [29]. Moreover, there is no P content

in boron derivative waste, too. According to chemical analysis results, obtained by X-ray fluorescence (XRF) in the prior study [15], boron derivative waste comprised only 0.02 wt.% P_2O_5 . As a result, the presenting of P in biominerization media is essential for bone-like apatite formation in the case of absence of P in wafer composition.

SEM micrographs were taken at higher magnification of coarse and fine wafers before and after immersion in LRS for 1, 3, 5, 7, 14, 21 and 28 days are given in Figs. 9 and 10. The primary calcite crystals could be easily observed on 3 days and 1 day for coarse and fine powder, respectively. For both powders, needle-like crystals became thicker and denser with the increment of the incubation period and a 3D-network was established after 21 days. The size of calcite crystals reached approximately 200–500 nm after 28 days. Even though the

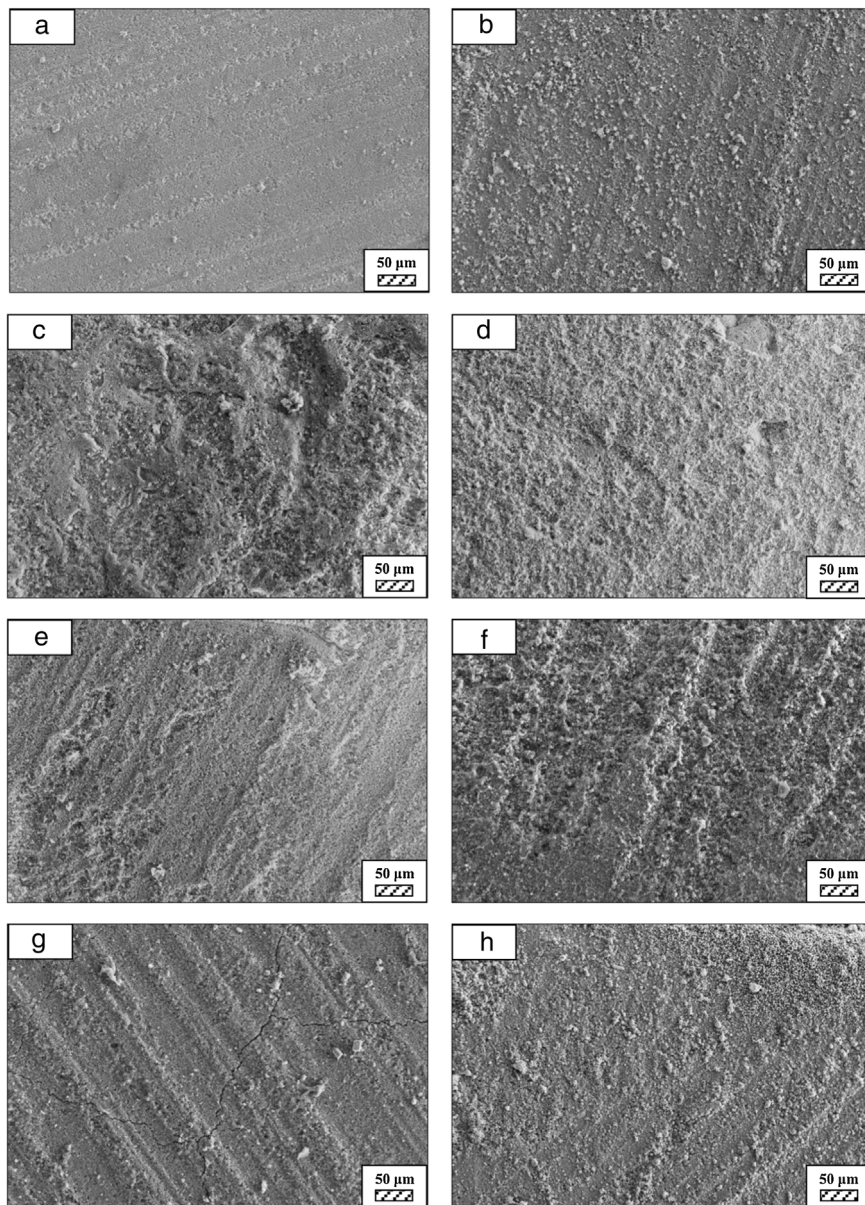


Fig. 12 – SEM micrographs of fine wafer before (a) and after immersion in HBP for (b) 1 day; (c) 3 days; (d) 5 days; (e) 7 days; (f) 14 days; (g) 21 days and (h) 28 days (500x).

calcite crystals on the surface of fine powder is thicker, the non-homogenously distribution of precipitate particles on the surface of fine powder could be a deficiency to obtain homogeneous osteoblast adhesion and osteoconductivity.

The researchers investigated the potential of CaCO_3 microparticles as templates for drug delivery applications by *in vitro* and *in vivo* experiments. The hydrophilic drugs, bioactive proteins, and DNA were adsorbed on the surface of CaCO_3 microparticles with the aim of solving the problems related to chemotherapy and radiotherapy [30]. For this reason, depending on the characteristics of precipitated CaCO_3 particles tailored during the incubation in LRS, SP-800 °C-4-h-crushed can have a potential for being used as bioactive bone graft substitutes and as drug delivery carriers in the field of tissue engineering and regenerative medicine.

In Human Blood Plasma

It is known that the formation of bone-like apatite layer on surface includes these steps: the exchange of alkali ions with hydrogen ions, the condensation of silanol (SiOH) groups, the polymerization of the SiO_2 -rich layer, the formation of an amorphous calcium phosphate layer, the crystallization of amorphous calcium phosphate layer to apatite layer [29,31]. The precipitation of Ca-P based crystalline layer on wafer surface from saturated biominerilization media (e.g. HBF, SBF, LRS, etc.) involves nucleation and growth stages [19].

SEM micrographs of coarse and fine wafers before and after immersion in HBP for 1, 3, 5, 7, 14, 21 and 28 days are given in Figs. 11 and 12. It is observed that both the number and size of precipitated particles on wafer surfaces increased

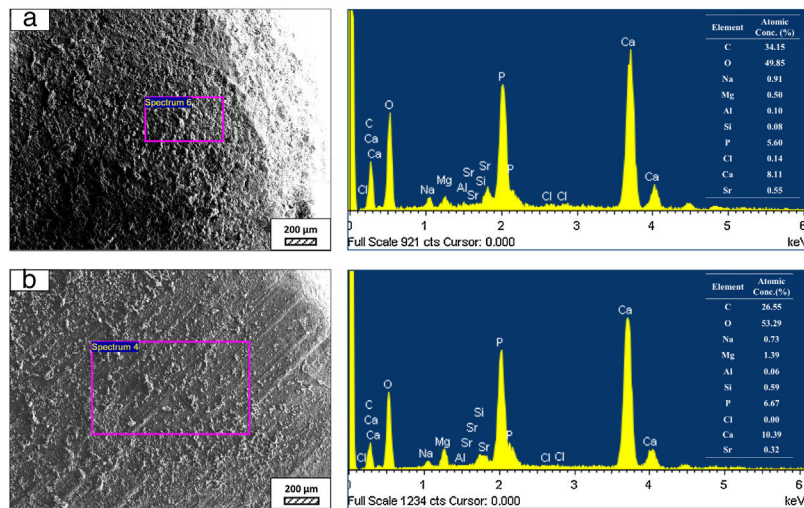


Fig. 13 – SEM micrographs and EDS analysis results of (a) coarse and (b) fine wafers soaked in HBP for 28 days.

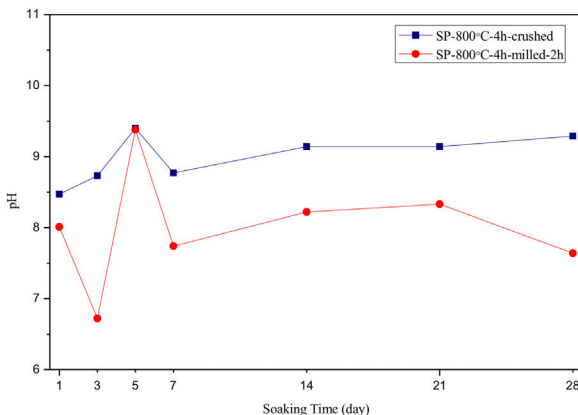


Fig. 14 – pH values of HBP with respect to immersion time.

with the incubation time. The precipitation could be first seen apparently on 5th days of incubation for coarse wafer and on 7th days for the fine wafer. SEM micrographs demonstrated that the surface roughness and open porosity of wafers increased by these incubation periods. The size range of precipitated particles was approximately 5–30 μm and 5–10 μm for coarse and fine wafers, respectively. Moreover, particles were distributed homogenously on the surface of the coarse wafer while the fine wafer surface did not homogenously cover by them. It points out that heterogeneous nucleation took place on a fine wafer surface. It was associated with lower surface roughness of fine wafers.

SEM micrographs and EDS analysis results of coarse and fine wafers soaked in HBP for 28 days are given in Fig. 13. The pH values of HBP with respect to immersion time are given in Fig. 14. Ca/P ratios on wafer surfaces with respect to immersion time are given in Fig. 15. SEM micrographs of coarse and fine wafers before and after immersion in HBP for 1, 3, 5, 7, 14, 21 and 28 days at higher magnification are given in Figs. 16 and 17. The presence of Ca and P in high

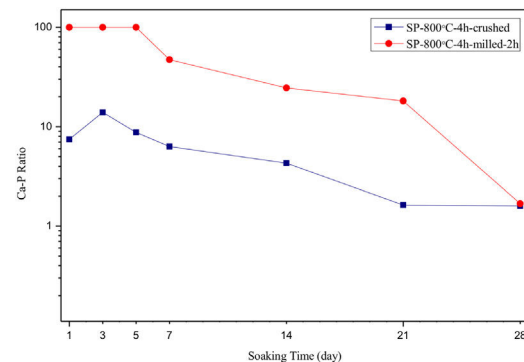


Fig. 15 – Ca/P ratios on wafer surfaces with respect to immersion time.

content indicates the formation of a bone-like apatite layer on the surface of monticellite based ceramic wafers after immersion in HBP for 28 days. On 28th days of immersion, Ca/P ratio was found 1.6 for coarse wafer and 1.68 for the fine wafer. These values showed that calcium-deficient hydroxyapatite ($\text{Ca}_{10-x}(\text{HPO}_4)_x(\text{PO}_4)_{6-x}(\text{OH})_{2-x}$ ($0 < x < 1$)) and stoichiometric hydroxyapatite ($\text{Ca}_{10}(\text{PO}_4)_6(\text{OH})_2$) layer was formed respectively, as a sign of bioactivity [32]. By contrast with LRS assessment, the pH values for coarse wafer were found higher for HBP test. This variety was associated with the difference of pH values of LRS (6.5) and HBP (7.4) where there is a significant difference in ion concentrations. An increase in pH values was observed at first days due to ion exchange of Ca^{2+} ions in wafers with H^+ in HBP which results in the formation of hydrated silica layer. After 5th days, pH sharply decreased owing to the apatite formation where OH^- ions in HBP were consumed [8]. In correlated with that, Ca/P ratio on wafer surfaces decreased (with the increment of P content) after 3rd and 5th days for coarse and fine wafers. SEM micrographs revealed that the formation of apatite became more obvious with denser crystalline layers with the increment of immersion time. The needle-like apatite crystals with

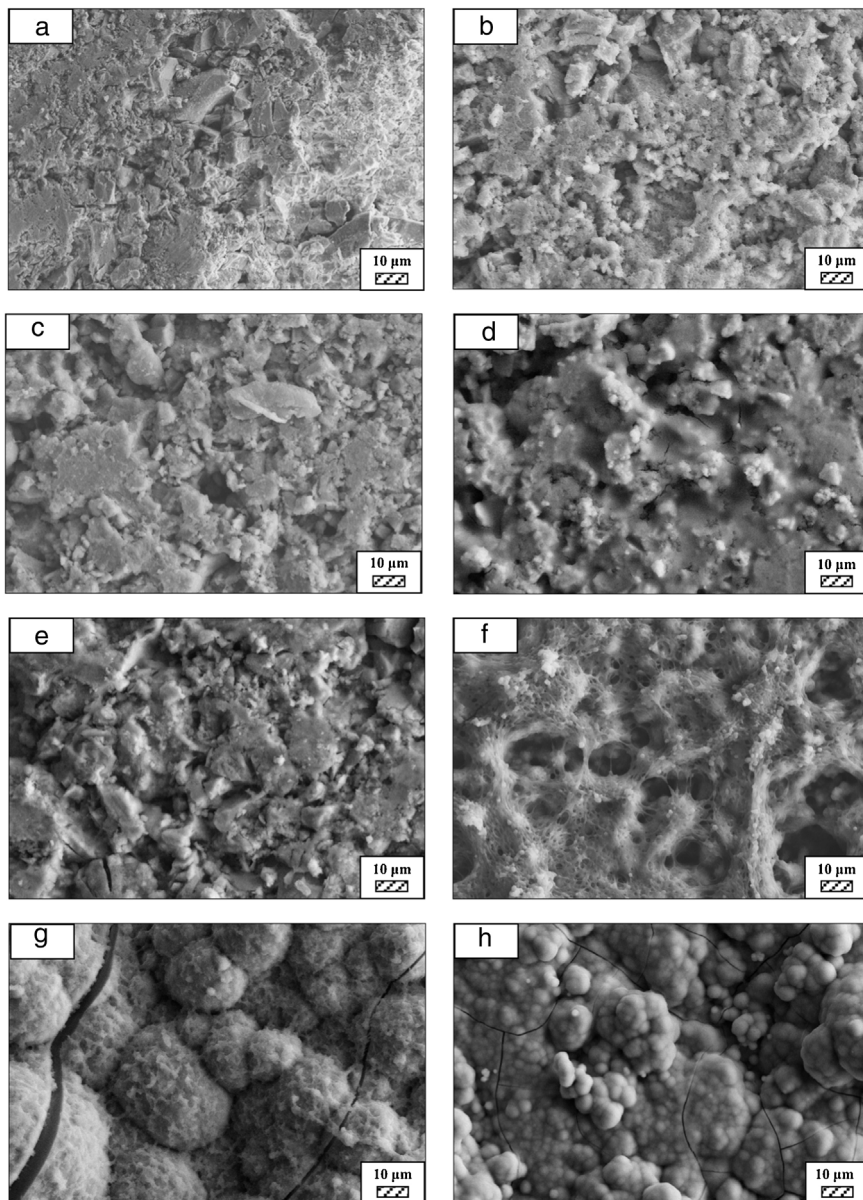


Fig. 16 – SEM micrographs of coarse wafer before (a) and after immersion in HBP for (b) 1 day; (c) 3 days; (d) 5 days; (e) 7 days; (f) 14 days; (g) 21 days and (h) 28 days (2500 \times).

a size lower than 5 μm could be easily observed on 14th days. The particles began to connect to each other through apatite crystals and a 3D-network has covered the surface up to 28 days.

In comparison with coarse wafer, the crystallite size was lower, and the surface of the fine wafer had not been homogeneously covered by apatite layer. Ca/P ratios on fine wafer surfaces in the first 5 days were determined roughly 100%. The P content in monticellite based wafers is nearly zero because boron derivative waste contains 0.02 wt% P_2O_5 according to XRF analysis [15]. In this situation, HBP is sole source for P content to provide Ca-P based apatite layer formation on the

surface. ~100% Ca/P ratio indicates that too low P content (between 0 and 1%) in HBP was able to be consumed for precipitation. On the other words, apatite crystallization on fine wafer surfaces took place after 5th day of incubation. Although, the degradation rate of the fine wafer was higher, the apatite formation kinetics was slower and non-homogenous distribution of apatite crystals on the surface was identified. As a result, the apatite formation was monitored by the particle size of powders. The higher surface roughness and higher specific surface area of coarse wafer resulted in a greater sticking probability for atoms favored the nucleation and growth kinetics of bone-like apatite formation [19].

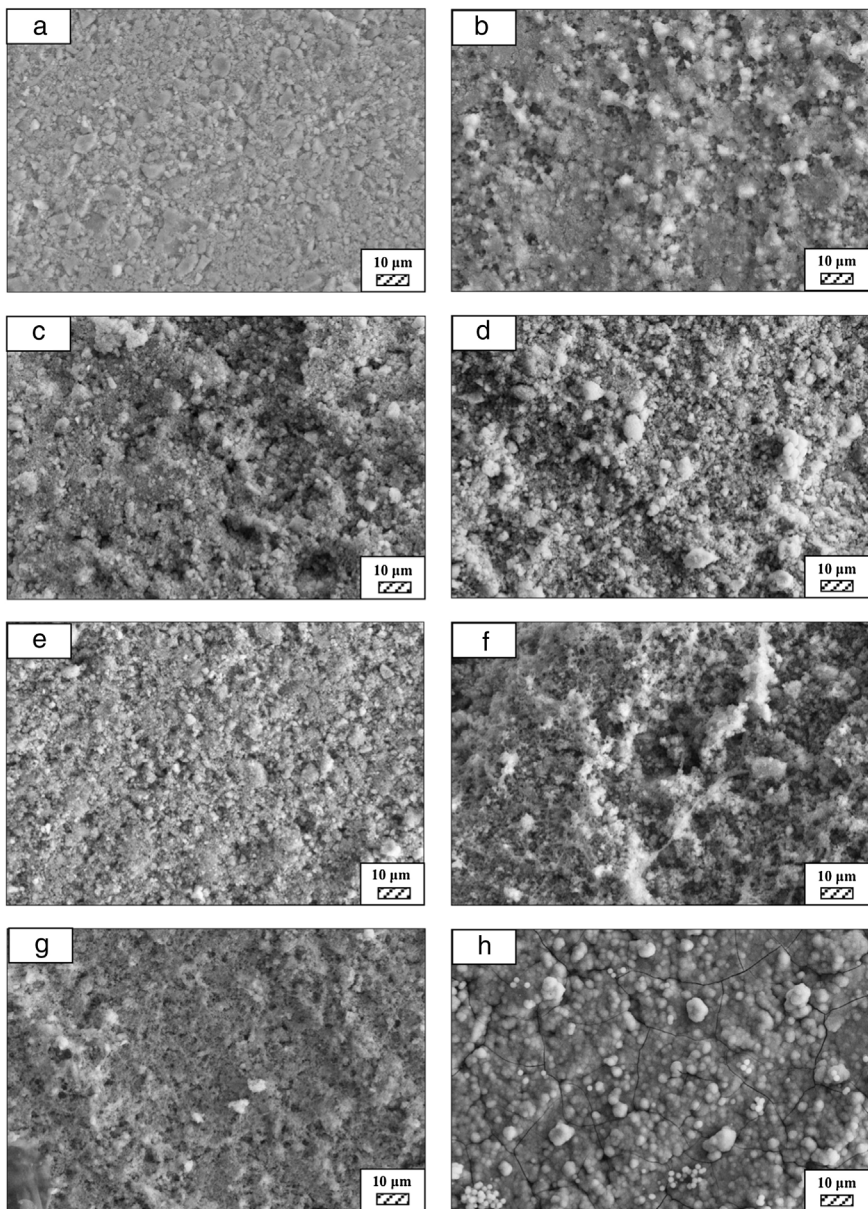


Fig. 17 – SEM micrographs of fine wafer before (a) and after immersion in HBP for (b) 1 day; (c) 3 days; (d) 5 days; (e) 7 days; (f) 14 days; (g) 21 days and (h) 28 days (2500 \times).

Conclusions

In the present study, monticellite based ceramic powder was synthesized using boron derivative waste at 800 °C for 4 h in an electrically heated furnace under atmospheric pressure. The synthesized powder was composed of monticellite, akermanite, diopside, calcium magnesium borate and zeolite LTA crystalline phases. MBCP was firstly crushed in an agate mortar and secondly ball-milled in ZrO₂ media under liquid-free environment. The amorphization of akermanite was increased with the increment of milling time above 2 h. The optimal milling time was selected as 2 h to obtain the

lowest average particle size and the narrowest particle size distribution. Next, *in vitro* bioactivity of coarse (d_{10} : 0.5 μ m, d_{50} : 3.0 μ m, d_{90} : 42 μ m) and fine (d_{10} : 0.5 μ m, d_{50} : 1.4 μ m, d_{90} : 4.8 μ m) monticellite based ceramic powders, obtained by crushing in an agate mortar and ball-milling for 2 h following to synthesis, were assessed by the immersion in Lactated Ringer's Solution and Human Blood Plasma for various periods (1, 3, 5, 7, 14, 21 and 28 days). The obtained results showed that

- calcite (CaCO_3) layer was formed on the surface of monticellite based ceramic wafers after immersion in Lactated Ringer's Solution for 28 days,

- if the host material is lack of P content, the existing of P in biominerization media is essential for bone-like apatite formation,
- in contrast to Lactated Ringer's Solution, calcium-deficient hydroxyapatite ($\text{Ca}_{10-x}(\text{HPO}_4)_x(\text{PO}_4)_{6-x}(\text{OH})_{2-x}$ ($0 < x < 1$)) and stoichiometric hydroxyapatite ($\text{Ca}_{10}(\text{PO}_4)_6(\text{OH})_2$) layer was formed on the surface of coarse and fine wafers, respectively after immersion in Human Blood Plasma for 28 days indicating good bioactive response,
- both calcite and bone-like apatite layer became denser with the increment of immersion time (from 1 to 28 days), however; crystals did not homogenously distribute on the smooth surface of fine wafers,
- the surface roughness of wafer favors homogeneous nucleation and growth kinetics of calcite and apatite precipitation.

Acknowledgments

This work was supported by the Scientific and Technological Research Council of Turkey (TÜBİTAK) [grant no. 116M218]. Authors thank Assoc. Prof. Dr. Erhan Ayas at the Department of Materials Science and Engineering in Eskisehir Technical University for his support on particle size reduction, and to Assoc. Prof. Dr. Hakan Gaşan at the Department of Metallurgical and Materials Engineering in Eskisehir Osmangazi University for his support on crystallite size measurements.

REFERENCES

- [1] M. Diba, O.M. Goudouri, F. Tapia, A.R. Boccaccini, Magnesium-containing bioactive polycrystalline silicate-based ceramics and glass-ceramics for biomedical applications, *Curr. Opin. Solid State Mater. Sci.* 18 (2014) 147–167, <http://dx.doi.org/10.1016/j.cossms.2014.02.004>.
- [2] K. Koch, D. Brave, A.A. Nasseh, A review of bioceramic technology in endodontics, *Bioceram. Technol.* 10 (2013) 6–13.
- [3] L.L. Hench, Bioceramics: from concept to clinic, *J. Am. Ceram. Soc.* 74 (1991) 1487–1510, <http://dx.doi.org/10.1111/j.1151-2916.1991.tb07132.x>.
- [4] S. Maitra, A. Rahaman, R. Pyare, H.B. Mukhtar, B.K. Dutta, Synthesis and characterization of bioactive-glass ceramics, *Adv. Bioceram. Porous Ceram. II* (2009) 83–94.
- [5] L.L. Hench, Bioceramics: research and development opportunities, *Braz. J. Phys.* 22 (1992) 70–84.
- [6] C. Wu, J. Chang, A novel akermanite bioceramic: preparation and characteristics, *J. Biomater. Appl.* 21 (2006) 119–129, <http://dx.doi.org/10.1177/0885328206057953>.
- [7] Y. Huang, X. Jin, X. Zhang, H. Sun, J. Tu, T. Tang, J. Chang, K. Dai, In vitro and in vivo evaluation of akermanite bioceramics for bone regeneration, *Biomaterials* 30 (2009) 5041–5048, <http://dx.doi.org/10.1016/j.biomaterials.2009.05.077>.
- [8] X. Chen, J. Ou, Y. Kang, Z. Huang, H. Zhu, G. Yin, H. Wen, Synthesis and characteristics of monticellite bioactive ceramic, *J. Mater. Sci. – Mater. Med.* 19 (2008) 1257–1263, <http://dx.doi.org/10.1007/s10856-007-3233-0>.
- [9] M.I.Z. Ridzwan, Problem of stress shielding and improvement to the hip implant designs: a review, *J. Med. Sci.* 7 (2007) 460–467.
- [10] X. Chen, J. Ou, Y. Wei, Z. Huang, Y. Kang, G. Yin, Effect of MgO contents on the mechanical properties and biological performances of bioceramics in the $\text{MgO}-\text{CaO}-\text{SiO}_2$ system, *J. Mater. Sci. – Mater. Med.* 21 (2010) 1463–1471, <http://dx.doi.org/10.1007/s10856-010-4025-5>.
- [11] F. Shamoradi, R. Emadi, H. Ghomi, Fabrication of monticellite-akermanite nanocomposite powder for tissue engineering applications, *J. Alloys Compd.* 693 (2017) 601–605, <http://dx.doi.org/10.1016/j.jallcom.2016.09.219>.
- [12] E. Kalantari, S.M. Naghib, M.R. Naimi-Jamal, M. Mozafari, Green solvent-based sol-gel synthesis of monticellite nanoparticles: a rapid and efficient approach, *J. Sol-Gel Sci. Technol.* 84 (2017) 87–95, <http://dx.doi.org/10.1007/s10971-017-4461-5>.
- [13] E. Kalantari, S.M. Naghib, N.J. Iravani, A. Aliahmadi, M.R. Naimi-Jamal, M. Mozafari, Nanostructured monticellite for tissue engineering applications – Part II: Molecular and biological characteristics, *Ceram. Int.* 44 (2018) 14704–14711, <http://dx.doi.org/10.1016/j.ceramint.2018.05.098>.
- [14] B. Cicek, Development of Glass-Ceramics from Combination of Industrial Wastes with Boron Mining Waste (Dissertation thesis), University of Bologna, Alma Mater Studiorum, 2013.
- [15] L. Koroglu, E. Ayas, A systematic study on solid-state synthesis of monticellite (CaMgSiO_4) based ceramic powders obtained from boron derivative waste, *Adv. Powder Technol.* 29 (2018) 2835–2844, <http://dx.doi.org/10.1016/j.apt.2018.08.003>.
- [16] L. Koroglu, E. Butev, Z. Esen, E. Ayas, A novel approach for synthesis of monticellite based bioactive ceramic powders from boron derivative waste, *Mater. Lett.* 209 (2017) 315–318, <http://dx.doi.org/10.1016/j.matlet.2017.08.034>.
- [17] B. Barutça, L. Körögülu, E. Ayas, A.T. Koparal, In vitro cytotoxicity of monticellite based bioactive ceramic powder synthesized from boron derivative waste, *Ceram. Int.* 44 (2018) 8094–8099, <http://dx.doi.org/10.1016/j.ceramint.2018.01.252>.
- [18] M. Mour, D. Das, T. Winkler, E. Hoenig, G. Mielke, M.M. Morlock, A.F. Schilling, Advances in porous biomaterials for dental and orthopaedic applications, *Materials* 3 (2010) 2947–2974, <http://dx.doi.org/10.3390/ma3052947>.
- [19] T.A. Ring, Fundamentals of Ceramic Powder Processing and Synthesis, second ed., Academic Press, San Diego, 1996.
- [20] M.S. El-Eskandarany, Mechanical Alloying: Nanotechnology, Materials Science and Powder Metallurgy, second ed., William Andrew Pub., MA, 2015.
- [21] X. Chatzistavrou, T. Zorba, K. Chrissafis, G. Kaimakamis, E. Kontonasaki, P. Koidis, K.M. Paraskevopoulos, Influence of particle size on the crystallization process and the bioactive behavior of a bioactive glass system, *J. Therm. Anal. Calorim.* 85 (2006) 253–259, <http://dx.doi.org/10.1007/s10973-005-7165-y>.
- [22] A.C. Tas, Submicron spheres of amorphous calcium phosphate forming in a stirred SBF solution at 55 °C, *J. Non-Cryst. Solids* 400 (2014) 27–32, <http://dx.doi.org/10.1016/j.jnoncrysol.2014.04.031>.
- [23] G. Kaur, G. Pickrell, G. Kimsawatde, D. Homa, H. Allbee, N. Sriranganathan, Synthesis, cytotoxicity, and hydroxyapatite formation in 27-Tris-SBF for sol-gel based $\text{CaO}-\text{P}_2\text{O}_5-\text{SiO}_2-\text{B}_2\text{O}_3-\text{ZnO}$ bioactive glasses, *Sci. Rep.* 4 (2014) 4392, <http://dx.doi.org/10.1038/srep04392>.
- [24] A.A. Ali, P. Baumli, G. Mucci, Mechanical alloying and milling in: Conference paper: MultiScience – XXIX. microCAD International Multidisciplinary Scientific Conference, 2015, <http://dx.doi.org/10.26649/musci.2015.017>.
- [25] A.G. King, Ceramic Technology and Processing, first ed., William Andrew-Noyes Publications, New York, 2002.
- [26] J. Park, Bioceramics: Properties, Characterization, and Applications, Springer, New York, 2008.

- [27] A. Monshi, M.R. Foroughi, M.R. Monshi, Modified Scherrer equation to estimate more accurately nano-crystallite size using XRD, *World J. Nano Sci. Eng.* 2 (2012) 154–160, <http://dx.doi.org/10.4236/wjNSE.2012.23020>.
- [28] T. Kokubo, H. Takadama, How useful is SBF in predicting *in vivo* bone bioactivity? *Biomaterials* 27 (2006) 2907–2915.
- [29] A.C. Tas, The use of physiological solutions or media in calcium phosphate synthesis and processing, *Acta Biomater.* 10 (2014) 1771–1792, <http://dx.doi.org/10.1016/j.actbio.2013.12.047>.
- [30] L.M. Manzine Costa, G.M. de Oliveira, R. Salomao, Precipitated calcium carbonate nano-microparticles: applications in drug delivery, *Adv. Tissue Eng. Regen. Med.* 3 (2) (2017) 336–340, <http://dx.doi.org/10.15406/atroa.2017.03.00059>.
- [31] L.L. Hench, Chronology of bioactive glass development and clinical applications, *New J. Glass Ceram.* 3 (2013) 67–73, <http://dx.doi.org/10.4236/nJGC.2013.32011>.
- [32] M. Santin, G. Phillips, *Biomimetic, Bioresponsive, and Bioactive Materials: An Introduction to Integrating Materials with Tissues*, John Wiley & Sons, Inc., New Jersey, 2012.